THE JOURNAL OF PHYSICAL CHEMISTRY C

pubs.acs.org/JPCC Article

# Formation of the Wrinkle Structure on a Styrene–Butadiene–Styrene Block Copolymer Surface by Surface Chemical Reformation via Ion-Beam Irradiation

Ju Hwan Lee,[⊥] Hae-Chang Jeong,[⊥] Jonghoon Won, Dong Hyun Kim, Dong Wook Lee, In Ho Song, Jin Young Oh, Dai-Hyun Kim, Yang Liu,* and Dae-Shik Seo*

Cite This: https://dx.doi.org/10.1021/acs.jpcc.0c00345 Read Online

ACCESS | Metrics & More | Article Recommendations

**ABSTRACT:** A styrene–butadiene–styrene (SBS) block copolymer was utilized to fabricate the wrinkle pattern in accordance with the buckling theory via ion-beam (IB) irradiation that induced surface reformation resulting in modulus mismatch and compressive strain. Using several analyses, different wrinkle patterns on the SBS surface were observed as the IB incidence angle was increased. After IB irradiation, a random labyrinth pattern was achieved at all IB incidence angles except for 15°, with which a less-formed wrinkle pattern was observed. Chemical analysis revealed that IB irradiation induced reformation of the surface chemical composition resulting in a stiff surface skin layer on the wrinkle pattern. The morphology of the wrinkle pattern was numerically and visually investigated, the results of which indicate that large wavelength and amplitude were achieved at high IB incidence angles. Through the buckling theory and the results of the surface analyses, the reason for this phenomenon was established: the IB incidence angle was the most important factor for determining the size of the wrinkle pattern on the SBS substrate. Consequently, it was verified that the wavelength and amplitude of the wrinkle pattern can be controlled by varying the IB incidence angle to the SBS substrate.

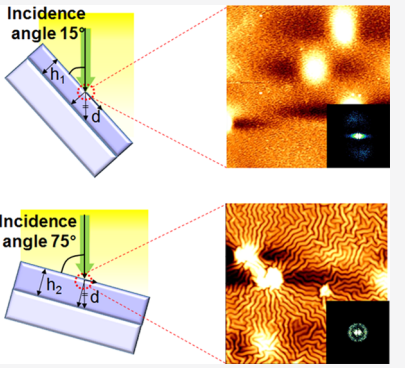


## 1. INTRODUCTION

In nature, wrinkles are commonly observed on various structures such as leaves, sea and cloud wave patterns, and the human skin.[1,2] This natural phenomenon (especially on the human skin) has inspired many researchers because wrinkles change the surface morphology and can improve the electrical, optical, biological, and mechanical properties of devices.[3−8] Thus, the fabrication of nano/microsized wrinkle patterns on the surface has been steadily investigated in a wide range of scientific researches, including stretchable electronics,[9−11] tunable surface wettability,[12,13] microfluidic channels,[14,15] liquid crystals alignment,[16,17] and biomaterials.[18,19] Modulus mismatch and external stimuli are required to fabricate wrinkle patterns on surfaces.[20,21]

As per the buckling theory, wavelength and amplitude are important measurements and several conditions must be fulfilled to fabricate a wrinkle pattern.[22−24] From the buckling theory, the wavelength ($\lambda$) and amplitude ($A$) can be described as

$$\lambda = 2\pi h\left(\frac{\bar{E}_f}{3\bar{E}_s}\right)^{1/3} \quad (1)$$

$$A = h\sqrt{\frac{\epsilon - \epsilon_c}{\epsilon_c}} \quad (2)$$

where $h$ is the thickness of the top (stiff) layer, $E_f$ and $E_s$ are the plane strain modulus values of the top (stiff) layer (film) and the substrate, respectively, $\epsilon$ is the compressive strain, and $\epsilon_c$ is the threshold critical strain, which can be estimated as $\epsilon_c \approx 0.25(3E_s/E_f)^{2/3}$.[25] According to the equations, the modulus mismatch between the top (stiff) layer and the elastomeric substrate ($E_f > E_s$) is the main factor causing a wrinkle pattern. In addition, when external stimuli are applied, compressive strain occurs, and a stress relief mechanism is induced between the top layer and the substrate. When the compressive strain exceeds the critical value ($\epsilon > \epsilon_c$), the effect of this phenomenon results in a wrinkle pattern on the surface. Several methods, such as plasma treatment,[26] metal deposition,[27] and ion-beam (IB) irradiation,[28] have been applied to

Received: January 14, 2020
Revised: March 24, 2020
Published: March 26, 2020

generate a stiff top layer. Among these, IB irradiation is a useful method that can generate a top (stiff) layer and apply external stimuli at the same time.

In many research studies, poly(dimethylsiloxane) (PDMS) has been used as an elastomeric substrate because it has attractive properties including low cost, flexibility, and the potential for various applications.[29−31] However, PDMS has a limitation when it is used to fabricate a fine wrinkle pattern, and so a change of material or process is required. The concept of using block copolymers (BCPs) is promising for producing smaller wrinkle patterns,[32,33] and although they are commonly used as self-assembly materials, it is possible to apply the buckling theory to fabricate wrinkle patterns on them. Thermoplastic rubbers such as styrene−butadiene−styrene (SBS) BCPs are strong candidates for wrinkle pattern production. SBS is composed of soft butadiene blocks and hard styrene blocks. The end-blocks (polystyrene) give strength to the polymer, whereas the midblocks (polybutadiene) provide remarkable elasticity.[34,35] Polystyrene behaves as a rubber-like elastomer below its glass transition temperature,[36] and even when SBS is heated above this temperature, its strength and elasticity are restored during the cooling process.[37]

In this study, we observed changes in the wrinkle pattern formed on SBS after exposure to IB irradiation as the IB incidence angle was increased from 15 to 75°. Field-emission scanning electron microscopy (FE-SEM) was conducted to identify the morphological changes of the surface, while chemical composition changes due to IB irradiation were verified using X-ray photoelectron spectroscopy (XPS) to investigate the reasons for the wrinkle formation. Furthermore, atomic force microscopy (AFM) was used to analyze specific information of the wrinkle pattern on the SBS and a two-dimensional fast Fourier transform (2D FFT) analysis was conducted to verify the distribution of the wrinkle pattern. A line-profile form AFM analysis was used to collect numerical information on the wrinkle pattern on SBS as a function of IB incidence angle. Through these analyses, the relationship between the formation of the wrinkle pattern and IB irradiation at various incidence angles was investigated.

## 2. MATERIALS AND METHODS

**2.1. Preparation of the SBS Samples on Glass Substrates.** SBS (styrene 21%, Figure 1) copolymer powder was dissolved in toluene to achieve 10 wt %. The SBS solution was stirred at 420 rpm and 65 °C for 2 h and then aged for at least 1 day. The prepared solution was spin-coated onto glass substrates (32 × 22 × 1.1 $mm^3$), as shown in Figure 2a. Before this process, the glass substrates were cleaned using acetone, methanol, and deionized (DI) water for 10 min each and then dried with $N_2$ gas. Spin-coating at 3000 rpm for 30 s was conducted to deposit the SBS solution on the glass substrates, after which they were cured at 75 °C for 1 h on a hot plate to remove the residual solvent on the surface (Figure 2b).

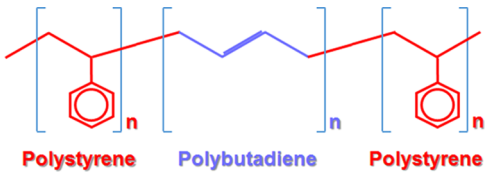


**Figure 1.** Chemical formula of the styrene−butadiene−styrene (SBS) block copolymer.

**2.2. IB Irradiation to Fabricate a Wrinkle Pattern on the SBS Surface.** The prepared SBS samples were placed in a vacuum chamber at a working pressure of 5 × $10^{-5}$ Torr with Ar gas flowing into the chamber with a rate of 1 sccm. The prepared SBS films were irradiated via an IB from an advanced DuoPIGatron-type IB system (Figure 2c). The IB irradiation conditions were 2400 eV for 1 min at incidence angles from 15 to 75° with increments of 15° ($10^4$−$10^5$ ions·$cm^{-2}$ in the IB current range of 0.9−1.1 mA·$cm^{-2}$). The IB incidence angle is the angle between the SBS surface and the IB irradiation direction, as shown in Figure 2c.

**2.3. Morphological Analysis of the Wrinkle Pattern on SBS Using FE-SEM.** The fabricated SBS surface wrinkle pattern (Figure 2d) due to IB irradiation was investigated via several analyses. The entire surface morphology of the SBS films was observed using FE-SEM (S-4200; Hitachi High-Technologies Corporation, Japan) as a function of IB incidence angle. The wrinkled structures were confirmed after enlarging the image of the surface 2000 times.

**2.4. Chemical Composition Investigation of SBS Wrinkle Pattern due to IB Irradiation.** XPS (K-Alpha, Thermo VG, U.K.) with a monochromatic Al X-ray source (Al K$\alpha$ line) was used to investigate the modification of the chemical structure of the SBS film surface before and after IB irradiation. The main chemical components of SBS (carbon and oxygen) were investigated.

**2.5. Specific Analysis of the Surface Wrinkled Structure Using AFM.** Specific information on the surface topology of the SBS film was measured via AFM (Park Systems, South Korea) with a scan size of 30 × 30 $\mu m^2$. AFM analysis was conducted in noncontact mode at a scan rate of 0.5 Hz. Moreover, 2D FFT analysis of the AFM image was conducted to characterize the wrinkle pattern size on the SBS film surface. Park Systems software with a line profile was used (XEI software, Park Systems) to investigate the changes in wavelength and amplitude of the wrinkle pattern on SBS at various IB incidence angles. The values of wavelength and amplitude were collected more than 15 times for the typical wrinkle patterns in the AFM images.

## 3. RESULTS AND DISCUSSION

Changes in the wrinkle morphology of the SBS surface as a function of IB incidence angle were observed via FE-SEM. Figure 3a presents the non-IB irradiated SBS surface morphology, and Figure 3b−f presents the SBS surface morphology at IB incidence angles from 15 to 75° with increments of 15°. Two interesting phenomena concerning the SBS surface morphology were found. First, when comparing before and after IB irradiation, the wrinkled structures on the SBS surface were observed only after IB irradiation, except for at an incidence angle of 15°. This indicates that IB irradiation induced an important effect on the SBS substrate surface that encourages the formation of the wrinkled structure. Second, a random labyrinth pattern was observed after IB irradiation (except for at an incidence angle of 15°) and the wrinkle pattern became clearer as the IB incidence angle was increased. This is because the wavelength of the wrinkle pattern was increased as the incidence angle was increased, indicating that the wavelength and the IB incidence angle are strongly correlated with each other. Furthermore, the labyrinth pattern


https://dx.doi.org/10.1021/acs.jpcc.0c00345
J. Phys. Chem. C XXXX, XXX, XXX−XXX

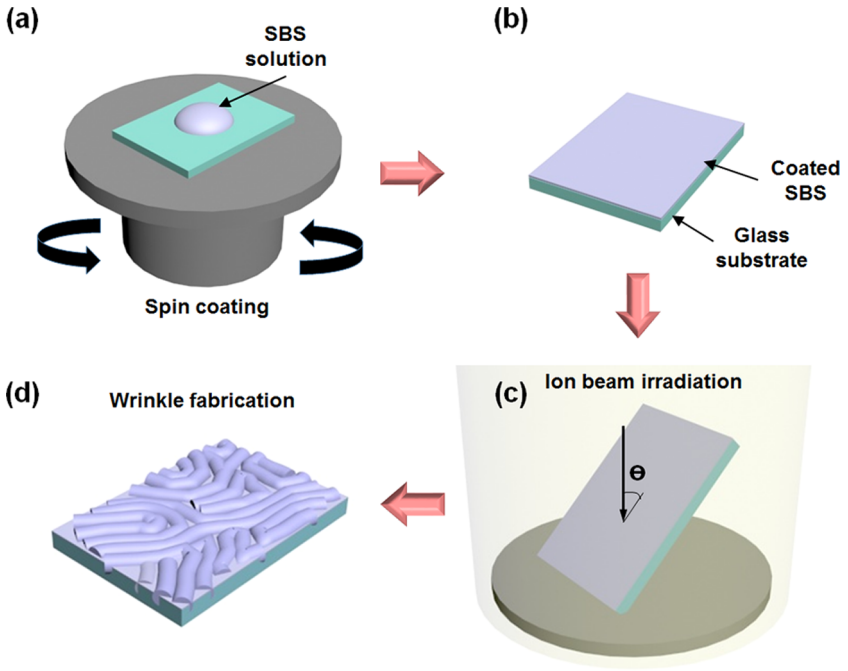


**Figure 2.** Schematic of wrinkle fabrication on SBS substrates. (a) Spin-coating of SBS solution onto a glass substrate at 3000 rpm for 30 s. (b) Fabricated SBS thin film cured at 75° for 1 h on a hot plate. (c) IB irradiation of the SBS surface at incidence angles from 15 to 75° with increments of 15°. (d) Wrinkled structure formation on the SBS surface.

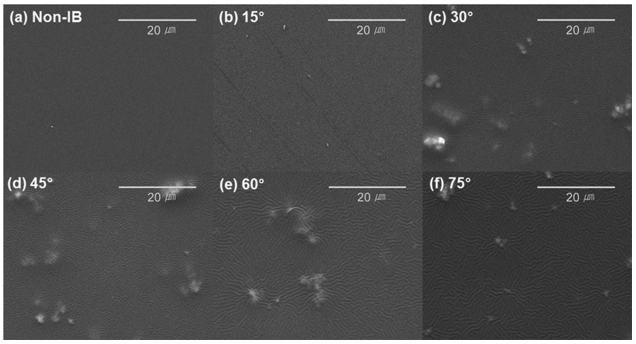


**Figure 3.** FE-SEM images of (a) a non-IB-irradiated SBS film surface and IB-irradiated SBS film surfaces at incidence angles of (b) 15°, (c) 30°, (d) 45°, (e) 60°, and (f) 75° (enlarged 2000 times).

on the SBS surface indicates that the change in IB incidence did not produce a one-dimensional striped wrinkle pattern.

Figure 4a illustrates the mechanism for the wrinkled structure on SBS in accordance with the foundational theory of wrinkle formation. Modulus mismatch between the bilayers due to the soft layer with a hard skin is required to fabricate a wrinkled structure. The soft substrate is expanded using an external force such as heat or mechanical stretching, and after deposition of the hard skin layer, contraction while releasing energy occurs, which forms the wrinkled structure. Because only a single material was used in this study, observations of the wrinkle formation on the surface indicate that a layer with a different modulus from SBS was induced after IB irradiation. Furthermore, it is obvious that IB irradiation reformed the surface with a higher modulus than bulk SBS. In principle, accelerated ions delivered by the IB system penetrate the

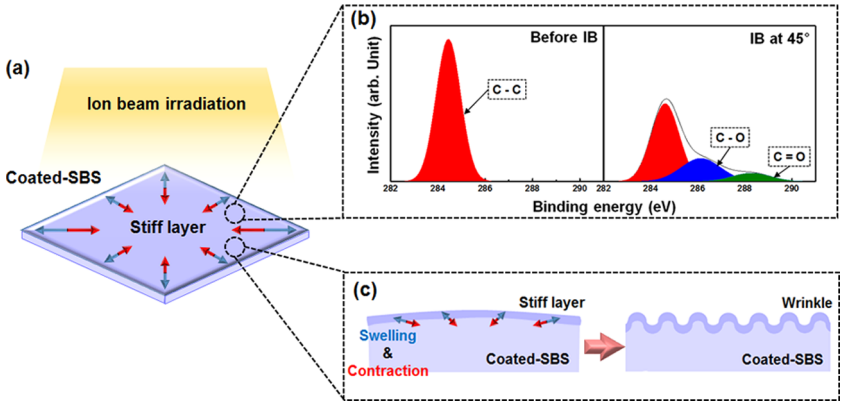


**Figure 4.** (a) Schematic of the wrinkle pattern formation on the top (stiff) layer of an SBS film surface due to IB irradiation. (b) XPS C 1s spectra of the SBS film surface before and after IB irradiation at an incidence angle of 45°. (c) Mechanism of wrinkle fabrication. IB irradiation induced a top (stiff) layer on the SBS surface via swelling and contraction forces (the blue and red arrows, respectively).



https://dx.doi.org/10.1021/acs.jpcc.0c00345
J. Phys. Chem. C XXXX, XXX, XXX−XXX

irradiated surface, thereby inducing chemical reformation by reactions such as surface oxidation.

To confirm this theory, XPS analysis of the SBS film surface was conducted to verify the chemical composition reformation due to IB irradiation. Figure 4b presents C 1s XPS spectra of the SBS film surface before and after IB irradiation at an incidence angle of 45°. As shown in Figure 1, SBS has phenyl groups but no oxygen bonds. Therefore, before IB irradiation, only one peak centered at 284.4 eV, indicating that carbon bonds in the SBS film surface were observed in the XPS spectrum. After IB irradiation at an incidence angle of 45°, two more peaks appeared in the XPS spectrum signifying carbon−oxygen single (C−O) bonds and carbon−oxygen double (C═O) bonds located at 286.1 and 288.3 eV, respectively. This result indicates that chemical bonds between carbon and oxygen were induced by IB irradiation. The C−C bond peak intensity decreased after IB irradiation, indicating that carbon bonds in the IB-irradiated SBS film surface had been broken, which caused the film surface to become unstable. To become stable once again, there was rebonding with nearby O atoms leading to increases in C−O and C═O bonds in the IB-irradiated SBS film during the reformation of the chemical composition of the SBS film surface. This phenomenon can be observed in the atomic composition ratios reported in Table 1.

**Table 1. Carbon and Oxygen Atomic Composition Ratios of the SBS Film Surface before and after IB Irradiation**

| elements | C (%) | O (%) |
|---|---|---|
| before IB | 95.12 | 4.88 |
| after IB | 78.69 | 21.31 |

Before IB irradiation, the atomic composition ratios of carbon and oxygen were 95.12 and 4.88%, respectively. After IB irradiation, the atomic composition ratio of carbon decreased to 78.69% whereas that of oxygen increased to 21.31%. From this, it was confirmed that the oxygen content increased in the SBS film surface after IB irradiation. Bonded O atoms acted as cross-linkers for the broken polymer chains caused by IB irradiation,[38] and thus a hardened skin layer was fabricated on the SBS film surface. Consequently, because of IB irradiation, a different chemical composition from the underlying SBS substrate was induced in the SBS film surface, and due to this, modulus mismatch occurred, which allowed the formation of the wrinkled structure.

Figure 4c shows the mechanism of wrinkle formation on the SBS film surface. Chemical composition reformation allowed the irradiated surface to obtain a high modulus, indicating a stiff layer, as is also suggested by the results of the previous analyses. During this process, ion collisions on the irradiated surface were induced and because of them, heat was generated that induced thermal volume expansion. In addition, after IB irradiation, the generated heat dissipated, and the swollen substrate contracted. Chemical reformation by IB irradiation changed not only the modulus but also the thermal expansion coefficient of the irradiated surface. This caused a difference in the volume expansion of the IB-irradiated surface and the SBS substrate caused by the generated heat. Due to swelling and contracting, compressive strain was induced on the surface on which the wrinkled structure formed when it exceeded the threshold critical strain $\varepsilon_c$ (eq 2). Consequently, these complex phenomena due to IB irradiation induced the wrinkled structure on the SBS surface. In addition, the overall direction of the compressive strain was verified by observing the labyrinth pattern. The orientation of the wrinkle pattern was determined by the distribution direction of the compressive strain on the stiff layer (along the landscape and portrait directions in the figure). Moreover, the applied external force needs to be released to end up with minimal elastic energy on the surface. When this occurs, the optimal pattern when releasing the energy is the wrinkle pattern,[38−40] and the compressive strain biased in one direction induces the wrinkle pattern aligned in the perpendicular direction. Thus, the random labyrinth pattern indicates that the compressive strain was distributed evenly in all directions. Furthermore, because a random labyrinth pattern was observed at all IB incidence angles, it is obvious that the change in incidence angle did not affect the direction of the compressive strain on the surface.

For the specific analysis of the wrinkled structure, an AFM image of the SBS surface was observed as a function of the IB incidence angle (Figure 5). Before IB irradiation (Figure 5a),

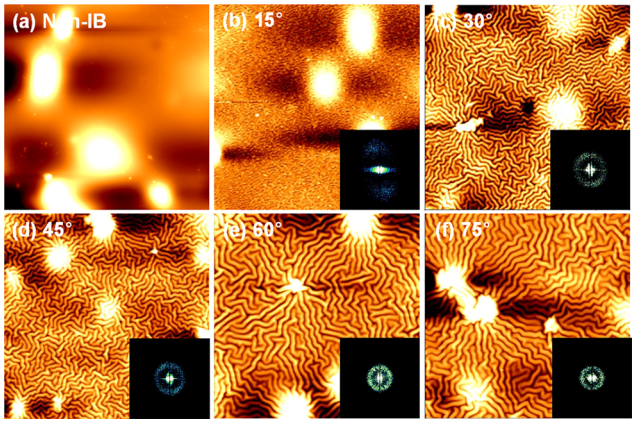


**Figure 5.** AFM images of (a) non-IB-irradiated SBS film surface and IB-irradiated SBS film surfaces at incidence angles of (b) 15°, (c) 30°, (d) 45°, (e) 60°, and (f) 75° with 2D-FFT pattern images for characterizing the formed wrinkle pattern.

no significant features were observed on the SBS substrate, which is the same as in the FE-SEM image. On the other hand, at an IB incidence angle of 15° (Figure 5b), a wrinkle pattern unlike the one observed in the FE-SEM image was observed, albeit less well-formed and different from the other incidence angles. Therefore, it seems that the reason for not observing wrinkle formation in Figure 3 is a complex phenomenon of a less-formed structure and electron beam damage of the polymer by FE-SEM while measuring the SBS surface. Furthermore, this result indicates that IB irradiation at an incidence angle of 15° was not enough to fabricate a well-formed wrinkled structure on the SBS surface. A clear wrinkle pattern can be clearly observed in the AFM image when the IB incidence angle was increased to 30° (Figure 5c). This indicates that IB irradiation at an incidence angle of 30° and above is appropriate for fabricating a well-formed wrinkle pattern. In addition, it can be clearly seen in the FE-SEM images that the size of the wrinkle pattern increased as the IB incidence angle was increased, and the highest wavelength was achieved at an IB incidence angle of 75° (Figure 5f). This indicates that the wavelength of the wrinkled structure on the SBS strongly depends on the IB incidence angle. In addition, the shape of the wrinkle pattern on SBS was also observed. Above an IB incidence angle of 30°, a generally random


https://dx.doi.org/10.1021/acs.jpcc.0c00345
J. Phys. Chem. C XXXX, XXX, XXX−XXX

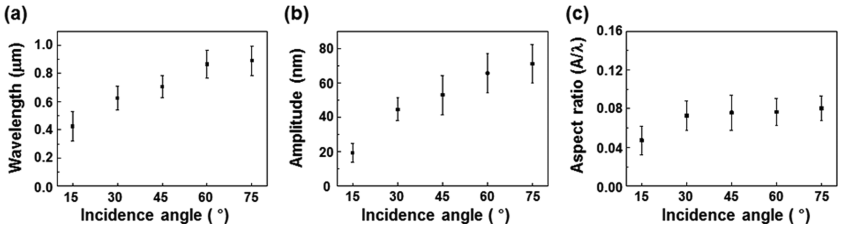


**Figure 6.** (a) Average wavelength, (b) average amplitude, and (c) aspect ratio of the wrinkle patterns on SBS as a function of IB incidence angle.

labyrinth pattern was observed. However, the AFM measurements were conducted on narrower sections than the FE-SEM measurements, and due to this, random labyrinth patterns were not clearly observed at IB incidence angles of 60 and 75°. Therefore, the surface characteristics of the SBS structures were identified using the 2D-FFT analysis, which converts the spatial information in the AFM image into 2D-FFT graphs in the spatial frequency domain defined by mathematical calculations. The distribution of the 2D-FFT graph (the bright parts in the images) indicates the periodicity of the SBS surface structure. Because the less well-formed wrinkle pattern at an IB incidence angle of 15° is not clear, the distribution on the 2D-FFT graph was biased in one direction. On the other hand, above an IB incidence angle of 15°, circle-like 2D-FFT graph distributions were achieved, which means that they were distributed equally in the spatial frequency domain. This indicates that the wrinkled structures on the SBS substrate were almost equally distributed, as confirmed by the random labyrinth pattern. Furthermore, the diameter of the circle-like 2D-FFT graph is based on the reciprocal of the average wrinkle wavelength. Thus, it can be observed that the diameter decreased as the IB incidence angle was increased, indicating that a high IB incidence angle resulted in a large wavelength in the wrinkled structure. These results visually reveal that the wrinkled structure on SBS at above an IB incidence angle of 15° had random labyrinth patterns and the largest wrinkle wavelength was achieved at an IB incidence angle of 75°.

The wavelength and amplitude values of the wrinkled structures on the SBS were collected by conducting a line profile analysis of the AFM measurements to investigate specific information of the wrinkle pattern size as a function of IB incidence angle (Figure 5); the collected average wavelength values of the wrinkled structures on SBS are presented in Figure 6a. The average wavelengths of the wrinkle pattern on the SBS were 0.425, 0.625, 0.706, 0.866, and 0.891 $\mu$m at incidence angles of 15, 30, 45, 60, and 75°, respectively. These values numerically confirm that the wavelength of the wrinkled structures on SBS increased as the IB incidence angle was increased (as shown in the FE-SEM and the AFM images). Furthermore, the average amplitude values as a function of IB incidence angle were also collected, as shown in Figure 6b; these were 19.194, 44.511, 52.886, 65.585, and 71.039 nm at incidence angles of 15, 30, 45, 60, and 75°, respectively (Table 2). The average amplitude values showed a similar tendency of increasing wavelength as the IB incidence angle was increased, indicating that IB irradiation on the SBS substrate with a high incidence angle induced high wavelength and amplitude. This demonstrates the controllability of the size of the wrinkle pattern on SBS by changing the IB incidence angle. Furthermore, it was verified that the wrinkle pattern on the SBS substrate had a smaller wavelength and amplitude than those reported for wrinkle patterns on PDMS under similar IB irradiation conditions.[39] As presented in Figure 6c, the aspect ratio ($A/\lambda$), which is the ratio of the wavelength to amplitude, at each IB incidence angle was calculated. The wrinkled structures on SBS at incidence angles of 15, 30, 45, 60, and 75° attained aspect ratios of 0.045, 0.073, 0.076, 0.076, and 0.080, respectively. Except for an IB incidence angle of 15°, with which a less-formed wrinkled structure was observed, nearly identical aspect ratios were achieved at all of the IB incidence angles. Using eqs 1 and 2, the aspect ratio of the wrinkled structure can be simply calculated as

**Table 2. Wavelength, Amplitude, and Aspect Ratio Values of the Wrinkle Patterns on SBS at Various IB Incidence Angles**

| IB incidence angle (deg) | wavelength ($\mu$m) | amplitude (nm) | aspect ratio |
|---|---|---|---|
| 15 | 0.425 | 19.194 | 0.045 |
| 30 | 0.625 | 45.511 | 0.073 |
| 45 | 0.706 | 52.886 | 0.075 |
| 60 | 0.866 | 65.585 | 0.076 |
| 75 | 0.891 | 71.039 | 0.080 |

$$\frac{A}{\lambda} \approx \frac{1}{\pi}(\Delta\varepsilon)^{1/2} = \frac{1}{\pi}\sqrt{\varepsilon - \frac{1}{4}\left(\frac{3E_s}{E_f}\right)^{2/3}} \quad (3)$$

where $\Delta\varepsilon = \varepsilon - \varepsilon_c$. In this equation, the compressive strain ($\varepsilon$) and substrate modulus ($E_s$) are fixed because of the constant application of IB irradiation energy and the same SBS substrate being used at all IB incidence angles in this study. Due to these fixed conditions, the aspect ratio of the wrinkled structure on SBS strongly depends on the surface modulus ($E_f$). Therefore, the change in surface modulus as the IB incidence angle was increased can be inferred using eq 3 and the collected aspect ratio values. Accordingly, it was confirmed that the SBS top (stiff) layer at an IB incidence angle of 15° had a relatively lower surface modulus than the others. At this incidence angle, the space between the SBS surface and the direction of IB irradiation was too narrow, so the IB did not irradiate the entire SBS surface evenly; this incurred insufficient chemical reformation of the irradiated surface, resulting in a stiff skin layer with a relatively low surface modulus value, and consequently, a less well-formed wrinkled structure was achieved. Nearly constant higher aspect ratios were achieved above an IB incidence angle of 15°. Through eq 3, it is obvious that there were no significant differences in the top (stiff) layer modulus values with an IB incidence angle above 15°, indicating that the IB irradiated the SBS surface evenly, which induced enough chemical reformation for fabricating a stiff skin layer to form the wrinkled structure. To sum up, it was confirmed through the line profile analysis that the size of the wrinkle pattern, including the wavelength and amplitude, can be controlled by changing the incidence angle, and the top (stiff) layer modulus was nearly constant above an IB incidence angle of 15°.


https://dx.doi.org/10.1021/acs.jpcc.0c00345
J. Phys. Chem. C XXXX, XXX, XXX−XXX

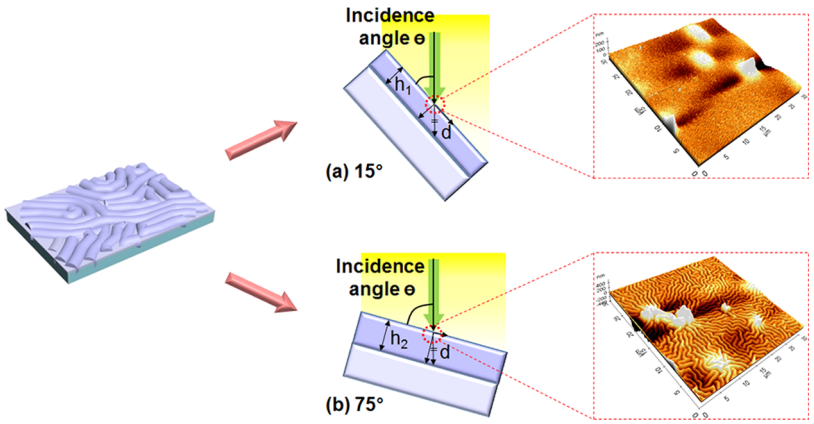


**Figure 7.** Schematic of IB irradiation on the SBS surface to determine the size of the wrinkle pattern at incidence angles of (a) 15° and (b) 75°. *d* is the penetration depth of the accelerated ions from the IB system and *h* is the thickness of the top (stiff) layer fabricated by IB irradiation.

Using eqs 1 and 2, and the results of the previous analyses, the reason for the change in the wrinkle pattern size on SBS was revealed as the increase in the IB incidence angle. However, above an IB incidence angle of 15°, the SBS surface had a nearly constant top (stiff) layer modulus value, as reported earlier. This indicates that the top (stiff) layer modulus was not a critical factor when determining the wrinkle pattern wavelength size as the IB incidence angle was increased. The wavelength of the wrinkle pattern is determined by the top (stiff) layer thickness (*h*) and modulus mismatch. Therefore, the wrinkle pattern wavelength strongly depended on *h*. Additionally, because constant IB irradiation energy was applied, the amplitude was largely determined by *h*. Schematics of IB irradiation on the SBS substrate at IB incidence angles of 15 and 75° are illustrated in Figure 7a,b, respectively. Ions accelerated by the IB system penetrate the irradiated substrate surface, with the penetration depth *d* being determined by the IB irradiation energy intensity. Therefore, for the same IB irradiation energy on the same substrate, a constant ion penetration depth is induced that according to the IB incidence angle, can be split in two directions: parallel to the substrate surface and perpendicular to it, with the latter becoming the thickness of the area affected by IB irradiation. As shown in Figure 3, IB irradiation induced a stiff skin layer via chemical reformation that became the top (stiff) layer (the thickness of which is denoted by *h* in Figure 7) that was determined by the angle between the IB irradiation direction and the SBS surface. Therefore, the thickness of the top (stiff) layer increased as the IB incidence angle was increased. Furthermore, applying eqs 1 and 2 revealed that the change in *h* with IB incidence angle was a critical factor for changing the size of the wrinkle pattern in terms of wavelength and amplitude, which were the largest at the highest IB incidence angle. To sum up the results of the analyses, it was confirmed that the controllability of the wavelength and amplitude using various IB incidence angles with the SBS substrate resulted in smaller wrinkles than reported with PDMS under the same conditions.

## 4. CONCLUSIONS

We controlled the wrinkle pattern size in terms of amplitude and wavelength by applying IB irradiation at various incidence angles. Furthermore, we confirmed the mechanism of wrinkle fabrication as the incidence angle was increased using FE-SEM, XPS, and AFM. Random labyrinth patterns were achieved on the SBS substrate above an incidence angle of 15°. However, at this low incidence angle, ions emitted from the IB system irradiated the surface unevenly, which resulted in a less-formed wrinkled structure on the surface. After the IB incidence angle was increased to above 15°, well-formed wrinkled structures were observed, indicating that a top (stiff) layer was induced on the SBS substrate and compressive strain was applied due to the even irradiation by the IB. It was confirmed via a chemical composition investigation that the original carbon bonds in the SBS were broken and new chemical bonds of carbon and oxygen were induced by IB irradiation, resulting in a wrinkled structure in the top (stiff) skin layer. Additionally, both numerical and visual analyses revealed that the size of the wrinkle pattern on the SBS in terms of wavelength and amplitude increased as the IB incidence angle was increased. Furthermore, using the aspect ratio confirmed that almost identical modulus values were achieved above an IB incidence angle of 15°. Hence, the size of the wrinkle pattern is affected by the thickness of the top (stiff) layer, which can be controlled by varying the IB incidence angle. Consequently, the controllability of wavelength and amplitude was ensured. Moreover, these values were smaller than on IB-irradiated PDMS under similar IB energy irradiation conditions.

## AUTHOR INFORMATION


### Corresponding Authors

**Yang Liu** − *College of Information Science and Technology, Donghua University, Shanghai 201620, China*; Email: liuyang@dhu.edu.cn

**Dae-Shik Seo** − *IT Nano Electronic Device Laboratory, Department of Electrical and Electronic Engineering, Yonsei University, Seoul 120-749, Republic of Korea*; orcid.org/0000-0002-6709-2996; Email: dsseo@yonsei.ac.kr

### Authors

**Ju Hwan Lee** − *IT Nano Electronic Device Laboratory, Department of Electrical and Electronic Engineering, Yonsei University, Seoul 120-749, Republic of Korea*

**Hae-Chang Jeong** − *Electrical Engineering, Changwon National University, Changwon, Gyeongnam 51140, Republic of Korea*

**Jonghoon Won** − *IT Nano Electronic Device Laboratory, Department of Electrical and Electronic Engineering, Yonsei University, Seoul 120-749, Republic of Korea*




https://dx.doi.org/10.1021/acs.jpcc.0c00345
J. Phys. Chem. C XXXX, XXX, XXX−XXX

**Dong Hyun Kim** − *IT Nano Electronic Device Laboratory, Department of Electrical and Electronic Engineering, Yonsei University, Seoul 120-749, Republic of Korea*
**Dong Wook Lee** − *IT Nano Electronic Device Laboratory, Department of Electrical and Electronic Engineering, Yonsei University, Seoul 120-749, Republic of Korea*
**In Ho Song** − *IT Nano Electronic Device Laboratory, Department of Electrical and Electronic Engineering, Yonsei University, Seoul 120-749, Republic of Korea*
**Jin Young Oh** − *IT Nano Electronic Device Laboratory, Department of Electrical and Electronic Engineering, Yonsei University, Seoul 120-749, Republic of Korea*
**Dai-Hyun Kim** − *Department of Smart Electric, Korea Polytechnic, Incheon 22121, Republic of Korea*

Complete contact information is available at: https://pubs.acs.org/10.1021/acs.jpcc.0c00345

### Author Contributions

⊥J.H.L. and H.-C.J. contributed equally to this work.

### Funding

National Research Foundation of Korea (Grant No. 2020-11-0234).

### Notes

The authors declare no competing financial interest.

## REFERENCES

(1) Wang, D.; Cheewaruangroj, N.; Li, Y.; McHale, G.; Jiang, Y.; Wood, D.; Biggins, J. S.; Xu, B. B. Spatially configuring wrinkle pattern and multiscale surface evolution with structural confinement. *Adv. Funct. Mater.* **2018**, *28*, No. 1704228.
(2) Park, S. K.; Kwark, Y.-J.; Nam, S.; Park, S.; Park, B.; Yun, S.; Moon, J.; Lee, J.-I.; Yu, B.; Kyung, K.-U. Wrinkle structures formed by formulating UV-crosslinkable liquid prepolymers. *Polymer* **2016**, *99*, 447−452.
(3) Kim, J.-H.; Yoneya, M.; Yokoyama, H. Tristable nematic liquid-crystal device using micropatterned surface alignment. *Nature* **2002**, *420*, 159−162.
(4) del Campo, A.; Arzt, E. Fabrication approaches for generating complex micro- and nanopatterns on polymeric surfaces. *Chem. Rev.* **2008**, *108*, 911−945.
(5) Biswas, A.; Bayer, I. S.; Biris, A. S.; Wang, T.; Dervishi, E.; Faupel, F. Advances in top−down and bottom−up surface nanofabrication: techniques, applications and future prospects. *Adv. Colloid Interface Sci.* **2012**, *170*, 2−27.
(6) Olivier, A.; Meyer, F.; Raquez, J.-M.; Damman, P.; Dubois, P. Surface-initiated controlled polymerization as a convenient method for designing functional polymer brushes: From self-assembled monolayers to patterned surfaces. *Prog. Polym. Sci.* **2012**, *37*, 157−181.
(7) Engel, Y.; Schiffman, J. D.; Goddard, J. M.; Rotello, V. M. Nanomanufacturing of biomaterials. *Mater. Today* **2012**, *15*, 478−485.
(8) Stafford, C. M.; Harrison, C.; Beers, K. L.; Karim, A.; Amis, E. J.; Vanlandingham, M. R.; Kim, H.-C.; Volksen, W.; Miller, R. D.; Simonyi, E. E. A buckling-based metrology for measuring the elastic moduli of polymeric thin films. *Nat. Mater.* **2004**, *3*, 545−550.
(9) Khang, D.-Y.; Jiang, H.; Huang, Y.; Rogers, J. A. A Stretchable form of single-crystal silicon for high-performance electronics on rubber substrates. *Science* **2006**, *311*, 208−212.
(10) Rogers, J. A.; Someya, T.; Huang, Y. Materials and mechanics for stretchable electronics. *Science* **2010**, *327*, 1603−1607.
(11) Ramuz, M.; Tee, B. C.-K.; Tok, J. B.-H.; Bao, Z. Transparent, optical, pressure-sensitive artificial skin for large-area stretchable electronics. *Adv. Mater.* **2012**, *24*, 3223−3227.
(12) Tian, D.; Song, Y.; Jiang, L. Patterning of controllable surface wettability for printing techniques. *Chem. Soc. Rev.* **2013**, *42*, 5184−5209.
(13) Kim, H. S.; Crosby, A. J. Solvent-responsive surface via wrinkling instability. *Adv. Mater.* **2011**, *23*, 4188−4192.
(14) Stroock, A. D.; Whitesides, G. M. Controlling flows in microchannels with patterned surface charge and topography. *Acc. Chem. Res.* **2003**, *36*, 597−604.
(15) Delamarche, E.; Bernard, A.; Schmid, H.; Michel, B.; Biebuyck, H. Patterned delivery of immunoglobulins to surfaces using microfluidic networks. *Science* **1997**, *276*, 779−781.
(16) Jeong, H.-C.; Park, H.-G.; Lee, J. H.; Jung, Y. H.; Jang, S. B.; Seo, D.-S. Homogeneous self-aligned liquid crystals on wrinkled-wall poly(dimethylsiloxane) via localised ion-beam irradiation. *Sci. Rep.* **2015**, *5*, No. 8641.
(17) Ohzono, T.; Fukuda, J. Zigzag line defects and manipulation of colloids in a nematic liquid crystal in microwrinkle grooves. *Nat. Commun.* **2012**, *3*, No. 701.
(18) Cho, J.-H.; Datta, D.; Park, S.-Y.; Shenoy, V. B.; Gracias, D. H. Plastic deformation drives wrinkling, saddling and wedging of annular bilayer nanostructures. *Nano Lett.* **2010**, *10*, 5098−5102.
(19) Cao, C.; Chan, H. F.; Zang, J.; Leong, K. W.; Zhao, X. Harnessing localized ridges for high-aspect-ratio hierarchical patterns with dynamic tunability and multifunctionality. *Adv. Mater.* **2014**, *26*, 1763−1770.
(20) Hou, H.; Yin, J.; Jiang, X. Reversible Diels−Alder reaction to control wrinkle patterns: from dynamic chemistry to dynamic patterns. *Adv. Mater.* **2016**, *28*, 9126−9132.
(21) Genzer, J.; Groenewold, J. Soft matter with hard skin: from skin wrinkles to templating and material characterization. *Soft Matter* **2006**, *2*, 310−323.
(22) Yang, S.; Khare, K.; Lin, P.-C. Harnessing surface wrinkle patterns in soft matter. *Adv. Funct. Mater.* **2010**, *20*, 2550−2564.
(23) Khang, D.-Y.; Rogers, J. A.; Lee, H. H. Mechanical buckling: mechanics, metrology, and stretchable electronics. *Adv. Funct. Mater.* **2009**, *19*, 1526−1536.
(24) Chung, J. Y.; Nolte, A. J.; Stafford, C. M. Surface wrinkling: a versatile platform for measuring thin-film properties. *Adv. Mater.* **2011**, *23*, 349−368.
(25) Moon, M.-W.; Lee, S. H.; Sun, J.-Y.; Oh, K. H.; Vaziri, A.; Hutchinson, J. W. Wrinkled hard skins on polymers created by focused ion beam. *Proc. Natl. Acad. Sci. U.S.A.* **2007**, *104*, 1130−1133.
(26) Breid, D.; Crosby, A. J. Effect of stress state on wrinkle morphology. *Soft Matter* **2011**, *7*, 4490.
(27) Bowden, N.; Brittain, S.; Evans, A. G.; Hutchinson, J. W.; Whitesides, G. M. Spontaneous formation of ordered structures in thin films of metals supported on an elastomeric polymer. *Nature* **1998**, *393*, 146−149.
(28) Evensen, H. T.; Jiang, H.; Gotrik, K. W.; Denes, F.; Carpick, R. W. Transformations in Wrinkle patterns: cooperation between nanoscale cross-linked surface layers and the submicrometer bulk in wafer-spun, plasma-treated polydimethylsiloxane. *Nano Lett.* **2009**, *9*, 2884−2890.
(29) Chiche, A.; Stafford, C. M.; Cabral, J. T. Complex micropatterning of periodic structures on elastomeric surfaces. *Soft Matter* **2008**, *4*, 2360−2364.
(30) Lee, W.-K.; Jung, W.-B.; Nagel, S. R.; Odom, T. W. Stretchable Superhydrophobicity from Monolithic, Three-Dimensional Hierarchical Wrinkles. *Nano Lett.* **2016**, *16*, 3774−3779.
(31) Khare, K.; Zhou, J.; Yang, S. Tunable open-channel microfluidics on soft poly(dimethylsiloxane) (PDMS) substrates with sinusoidal grooves. *Langmuir* **2009**, *25*, 12794−12799.
(32) Park, C.; Yoon, J.; Thomas, E. L. Enabling nanotechnology with self-assembled block copolymer patterns. *Polymer* **2003**, *44*, 6725−6760.
(33) Deng, T.; Ha, Y.-H.; Cheng, J. Y.; Ross, C. A.; Thomas, E. L. Micropatterning of block copolymer solutions. *Langmuir* **2002**, *18*, 6719−6722.

(34) Yu, J.; Wang, L.; Zeng, X.; Wu, S.; Li, B. Effect of montmorillonite on properties of styrene−butadiene−styrene copolymer modified bitumen. *Polym. Eng. Sci.* **2007**, *47*, 1289−1295.
(35) Romero-Sánchez, M. D.; Pastor-Blas, M. M.; Martín-Martínez, J. M.; Walzak, M. J. Addition of ozone in the UV radiation treatment of a synthetic styrene-butadiene-styrene (SBS) rubber. *Int. J. Adhes. Adhes.* **2005**, *25*, 358−370.
(36) Bianchi, U.; Pedemonte, E.; Turturro, A. Morphology of styrene-butadiene-styrene block copolymers. *Polymer* **1970**, *11*, 268−276.
(37) Airey, G. D. Rheological properties of styrene butadiene styrene polymer modified road bitumens. *Fuel* **2003**, *82*, 1709−1719.
(38) Jeong, H.-C.; Won, J.; Lee, J. H.; Mun, H.-Y.; Kim, D. H.; Lee, D. W.; Oh, B.-Y.; Han, J.-M.; Seo, D.-S. Homogeneously aligned liquid crystal molecules on unidirectional buckle pattern of polyurethane films. *Liq. Cryst.* **2018**, *45*, 95−101.
(39) Lin, P.-C.; Yang, S. Spontaneous formation of one-dimensional ripples in transit to highly ordered two-dimensional herringbone structures through sequential and unequal biaxial mechanical stretching. *Appl. Phys. Lett.* **2007**, *90*, No. 241903.
(40) Park, H.-G.; Jeong, H.-C.; Jung, Y. H.; Seo, D.-S. Control of the wrinkle structure on surface-reformed poly(dimethylsiloxane) via ion-beam bombardment. *Sci. Rep.* **2015**, *5*, No. 12356.


https://dx.doi.org/10.1021/acs.jpcc.0c00345
J. Phys. Chem. C XXXX, XXX, XXX−XXX